# Strained-Layer Relaxation in fcc Structures via the Generation of Partial Dislocations

D. M. Hwang, S. A. Schwarz, T. S. Ravi, R. Bhat, and C. Y. Chen
*Bellcore, Red Bank, New Jersey 07701*
(Received 26 October 1990)

A new strain-relief mechanism in strained III-V semiconductor structures is identified. The signature defect of the proposed mechanism is a microtwin along the {111} plane spanning an embedded strained layer. This defect can form when two partial dislocations with antiparallel Burgers vectors of the $\frac{1}{6}\langle 112\rangle$ type are generated inside the strained layer and glide to the opposite interfaces, leaving a stacking fault between them. This is a low-energy strain-relaxation channel and poses fundamental limitations for strained-layer device structures.

PACS numbers: 68.55.—a, 61.16.Di, 68.60.Dv, 81.15.Gh

Epitaxial growth of lattice-mismatched heterojunctions is of increasing importance for electronic and optoelectronic device fabrication. For thin epitaxial layers, the lattice mismatch may be accommodated by the distortion of the unit cells, resulting in strained pseudomorphic structures.[1] When the thickness of a strained layer exceeds a critical value, misfit dislocations[1] are formed at the interfaces to relieve the strain energy and the electrical and optical properties of the strained layer are catastrophically degraded. Much research[2-9] is aimed at understanding the dynamics of the defect-generating mechanism and predicting the critical thickness. However, the proper expressions for the misfit dislocation energy and the activation energy of the relaxation process are still controversial. Theoretical and experimental values of critical layer thickness are scattered over a wide range. For fcc systems, the most extensively studied structures of metals and semiconductors, the misfit dislocations considered[3-9] in critical thickness calculations are always perfect dislocations of the $\frac{1}{2}\langle 110\rangle$ type. Stacking faults and microtwins, although frequently observed in heteroepitaxial systems, are generally regarded as grown-in faults, not the result of strain relaxation.

We have studied[10-13] strain buildup and relaxation in $InP/In_{0.53}Ga_{0.47}As$ superlattices induced by Zn diffusion. The as-grown superlattices are lattice matched, free of strain and defects. In diffusion of Zn ions enhances the interdiffusion of the cations, In and Ga, while leaving the anions, P and As, relatively unaffected. The resulting superlattices are no longer lattice matched and frequently exhibit[11-13] microtwins along the {111} planes, spanning the thin As layers. These twin segments are not grown-in defects since they are not detected in the as-grown specimens. We have therefore suggested[11] that these microtwins are the result of strain relaxation.

In this Letter, we analyze the formation mechanism of stacking faults and microtwins in embedded strained layers of fcc structures and conclude that formation of stacking faults and microtwins is an energy-favorable strain-relaxation channel. We report the results of another strained system: AlAs layers embedded in InP and/or $In_{0.53}Ga_{0.47}As$. Stacking faults and microtwins are found to span AlAs layers of 4 and 5 nm in thickness. We propose that a pair of partial dislocations of the $\frac{1}{6}\langle 112\rangle$ type with antiparallel Burgers vectors can be generated inside an embedded strained layer and glide to the opposite interfaces, leaving a stacking fault between them. A series of partial dislocations can combine to form a microtwin several monolayers thick. High-resolution transmission-electron-microscopy (TEM) results substantiate this atomic model. For the relaxation of an embedded strained layer of material with small stacking-fault energy, we show that the formation of a pair of partial dislocations with their associated stacking fault is an energetically favored strain-relaxation channel, as compared with the formation of two perfect dislocations in the conventional[3] double-kink model. Therefore, the strain-relief mechanism proposed here poses fundamental limitations for strained-layer device structures.

Pristine unstrained $InP/In_{0.53}Ga_{0.47}As$ superlattices and strained AlAs layers embedded in InP and/or $In_{0.53}Ga_{0.47}As$ were fabricated by organometallic chemical vapor deposition on undoped InP substrates of [001] orientation. The InP and $In_{0.53}Ga_{0.47}As$ layers were grown at 625 °C while the AlAs layers were grown at 650 °C. TEM analysis of the cross-sectioned samples was performed using a JEOL 4000FX microscope operated at 400 keV.

A superlattice consisting of twenty periods of InP (40 nm) and $In_{0.53}Ga_{0.47}As$ (10 nm) was prepared. The as-grown superlattice was pseudomorphic, free of strain and defects.[10,11] After a 600 °C 1-h treatment in an evacuated sealed quartz ampoule with a $Zn_3As_2$ powder source, most of the superlattice was cation homogenized, yielding $In_{0.9}Ga_{0.1}P/In_{0.9}Ga_{0.1}As$ with a 3.2% lattice mismatch.[11] The top few P layers were converted into $Zn_3P_2$ with a sharp front as shown in Fig. 1. The $Zn_3P_2$ regions are easily identified in this medium-resolution TEM micrograph by the 0.8-nm × 1.2-nm lattice fringes, reflecting the superstructure of $Zn_3P_2$ which is a $\sqrt{2}\times\sqrt{2}\times 2$ arrangement of the zinc-blende unit cells.[11] There

© 1991 The American Physical Society

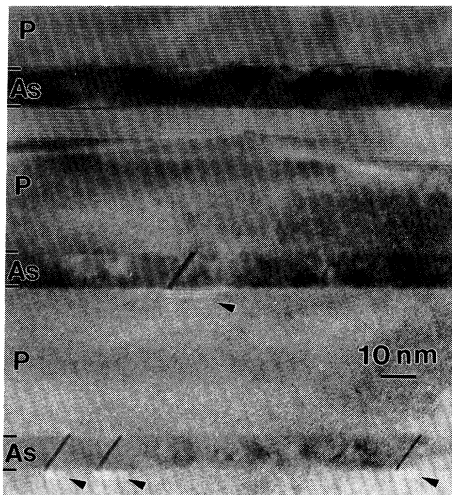


FIG. 1. TEM bright-field image taken along the $[1\bar{1}0]$ direction of an $InP/In_{0.53}Ga_{0.47}As$ superlattice after a 600 °C 1-h $Zn_3As_2$ treatment in a sealed ampoule. This micrograph shows a sharp front of $Zn_3P_2$ with 0.8-nm × 1.2-nm lattice fringes and the existence of $Zn_3P_2$ islands beyond the front as pointed by arrows. Adjacent to each $Zn_3P_2$ island is a microtwin spanning the 10-nm As layer.

exist some $Zn_3P_2$ islands beyond the continuous $Zn_3P_2$ front, located inside the P layers next to the upper interfaces. We speculate[11] that these islands are due to extra Zn dissolved in $In_{1-x}Ga_xP$ during the thermal treatment which then segregates into $Zn_3P_2$ islands along the colder faces of the P layers upon cooling. An observation of particular interest in Fig. 1 is that, for each $Zn_3P_2$ island, there exists a microtwin in the adjacent As layer. These microtwins, spanning the 10-nm As layers along the {111} planes, show up distinctly in TEM micrographs of diffraction contrast. High-resolution lattice-imaging studies indicated that these microtwins are one to three monolayers thick. Away from the $Zn_3P_2$ islands, the $In_{0.9}Ga_{0.1}P/In_{0.9}Ga_{0.1}As$ interfaces (with a 3.2% lattice mismatch) are defect free; no edge dislocations are detected. Since the as-grown specimen is pseudomorphic, these microtwins must be the result of strain relaxation. Apparently, the 4.8% lattice mismatch[11] between $Zn_3P_2$ and $In_{0.9}Ga_{0.1}As$ results in a critical layer thickness less than 10 nm and causes the 10-nm $In_{0.9}Ga_{0.1}As$ layers to relax partially.

Stacking faults and microtwins have been frequently observed in many heteroepitaxial systems. For example, Fig. 2 is a micrograph of a 5-nm AlAs layer sandwiched between InP and $In_{0.53}Ga_{0.47}As$ which also exhibits microtwins in the {111} planes. A high-resolution lattice image of one of the microtwins is shown in Fig. 3. This is a monolayer microtwin (two twinning operation separated by a monolayer) which can also be regarded as an intrinsic stacking fault.[14] No other defects, such as

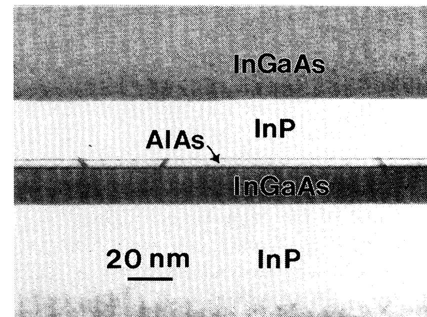


FIG. 2. TEM dark-field image taken along the $[1\bar{1}0]$ direction of a 5-nm AlAs layer embedded between InP and $In_{0.53}Ga_{0.47}As$. Microtwins spanning the AlAs layer are observable.

edge dislocations of the $\frac{1}{2}\langle 110\rangle$ type, have been detected in this specimen. AlAs has a lattice constant 3.5% smaller than that of InP or $In_{0.53}Ga_{0.47}As$. Since these microtwins extend from one strained interface to the other, they must be the result of strain relaxation after the AlAs layer has been capped. If these microtwins were growth faults, there is no mechanism to terminate them exactly at the other interface.

The stacking fault shown in Fig. 3 is terminated at both the upper and lower interfaces with partial dislocations of the $\frac{1}{6}\langle 112\rangle$ type. This configuration differs from that of the extended dislocation[14] which consists of a partial-dislocation pair resulting from the dissociation of a perfect dislocation, e.g., $\frac{1}{2}[\bar{1}01] \rightarrow \frac{1}{6}[\bar{1}\bar{1}2] + \frac{1}{6}[\bar{2}11]$, as shown in Fig. 4. The latter two partial dislocations repel each other since their Burgers vectors form an acute angle. Their separation is held at an equilibrium distance in balance with the stacking-fault energy.[14] A Burgers circuit around such an extended fault will result in a Burgers vector of $\frac{1}{2}[\bar{1}01]$. In contrast, a Burgers

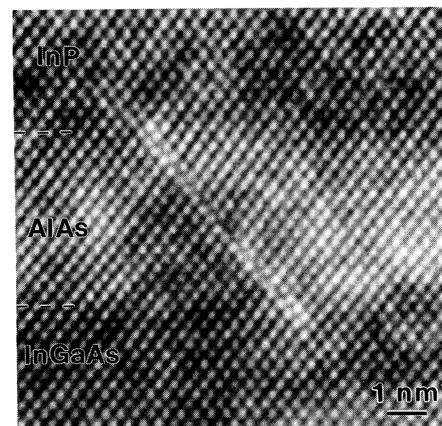


FIG. 3. High-resolution lattice image for the AlAs layer shown in Fig. 2. It shows an intrinsic stacking fault which can also be regarded as a monolayer-thick microtwin.

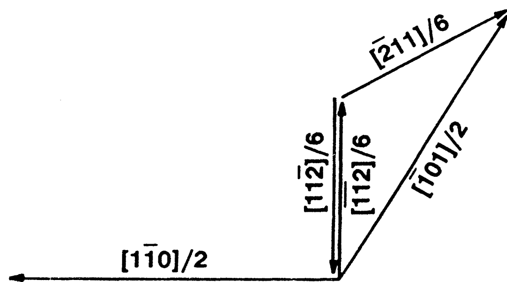


FIG. 4. Burgers vectors in a (111) plane of an fcc system for the $\frac{1}{2}\langle 110\rangle$-type perfect dislocations and the $\frac{1}{6}\langle 112\rangle$-type partial dislocations. The stacking fault shown in Fig. 3 is bounded by two partial dislocations with antiparallel Burgers vectors, e.g., $\frac{1}{6}[\bar{1}\bar{1}2]$ and $\frac{1}{6}[11\bar{2}]$.

circuit around the whole stacking fault shown in Fig. 3 results in a null Burgers vector. Therefore, the Burgers vectors at opposite ends of the stacking fault must be antiparallel to each other, e.g., $0 \rightarrow \frac{1}{6}[\bar{1}\bar{1}2]+\frac{1}{6}[11\bar{2}]$, as shown in Fig. 4. Note that, across the interfaces shown in Fig. 3, the bonds of the *ABA* stacking fault change their orientation continuously over a few unit cells and become the bonds of *ABC* stacking. This type of partial-dislocation pair is not in a metastable configuration and cannot exist in crystals which are unstrained, homogeneously strained, or with strain varying monotonously in one direction, since antiparallel dislocations attract each other and would annihilate immediately. In the system of embedded strained layers described here, these partial dislocations are generated and kept apart by the strain fields with local extrema.

The commonly discussed interface misfit dislocations in fcc systems are of the $\frac{1}{2}\langle 110\rangle$ type. There are three different perfect dislocations of the $\frac{1}{2}\langle 110\rangle$ type with Burgers vectors in a (111) plane, namely, $\frac{1}{2}[1\bar{1}0]$, $\frac{1}{2}[01\bar{1}]$, and $\frac{1}{2}[\bar{1}01]$. Two of them are shown in Fig. 4. Considering the growth direction along the [001] axis, the most frequently observed misfit dislocations in uncapped strained layers have Burgers vectors of $\frac{1}{2}[1\bar{1}0]$ in the interface plane, so-called Lomer dislocations. They are the most effective strain-relieving dislocations; each one relieves an in-plane strain of $a/\sqrt{2}$, where $a$ is the lattice parameter. However, a Lomer misfit dislocation cannot glide into or out of the strained interface since a dislocation can only glide in the plane containing both its line and its Burgers vector. The dislocations with Burgers vectors of $\frac{1}{2}[01\bar{1}]$ and $\frac{1}{2}[\bar{1}01]$, making a 60° angle with the dislocation line direction, say, $[1\bar{1}0]$, can glide from the free surface to the strained interface. These 60° misfit dislocations are less effective in strain relief; each one relieves a strain of $a/2\sqrt{2}$ along the [110] direction. It is believed that the relaxation of a strained layer is due to the gliding of 60° dislocations and the observed Lomer dislocation is the result of the interaction of 60° dislocations, e.g., $\frac{1}{2}[01\bar{1}]+\frac{1}{2}[\bar{1}01]\rightarrow\frac{1}{2}[\bar{1}10]$.

When a strained layer is capped with a thick unstrained layer, there is no strain field to promote dislocation gliding through the cap layer. Edge dislocations can still be formed at the strained interfaces by the bowing of threading dislocation or the expansion of microdislocation loops inside the strained layers, as described in the conventional[3] double-kink model. This requires the formation of two 60° dislocations on the two opposite interfaces of the strained layer in order to relieve a strain of $a/2\sqrt{2}$. Since it takes only one 60° dislocation to relieve the same amount of strain in an uncapped layer, it has been proposed[3,7,9] that a capped strained layer is more stable (i.e., with a larger critical thickness) than an uncapped layer. This would permit fabrication of overstrained embedded layers by "metastable" low-temperature epitaxy.

Our experimental observations, however, indicate that a capped strained layer can relax via the formation of partial dislocations. The projection of $\frac{1}{6}[\bar{1}\bar{1}2]$ on [110] yields $1/3\sqrt{2}$. This means that a $\frac{1}{6}[\bar{1}\bar{1}2]$ partial dislocation can relieve a strain $\frac{2}{3}$ (or a strain energy $\frac{4}{9}$) that of a 60° $\frac{1}{2}[\bar{1}01]$ perfect dislocation, for both dislocation lines along $[1\bar{1}0]$ and strain relief along [110]. Since the dislocation energy is approximately proportional to the square of the Burgers vector, the dislocation energy of a pair of $\frac{1}{6}\langle 112\rangle$ partial dislocations is $\frac{1}{3}$ that of a pair of $\frac{1}{2}\langle 110\rangle$ perfect dislocations, if the energy of the stacking fault between the partial dislocations is negligibly small. Comparing the partial-dislocation pair described here to the conventional 60°-perfect-dislocation pair, the former takes $\frac{1}{3}$ of the dislocation energy to form but relieves $\frac{4}{9}$ of the strain energy. In other words, the energy required to generate a pair of perfect dislocations can generate three pairs of partial dislocations. These three partial-dislocation pairs can relieve a total strain energy 33% more than that of a perfect-dislocation pair. Furthermore, the partial dislocations can be generated in a successive manner with small activation energy. Therefore, relaxation via the formation of partial dislocations is energetically favored for embedded strained layers.

The frequent observation of 60° perfect dislocations in uncapped strained layers may be due to the presence of free surfaces. Since a free surface is easy to deform in the out-of-plane direction, the out-of-plane component of a Burgers vector should contribute less than the in-plane component to the dislocation energy. A 60° perfect dislocation has a large out-of-plane component and its energy may be reduced substantially near a free surface. Therefore, the formation of 60° perfect dislocations may become favorable for uncapped strained layers.

To estimate the critical layer thickness of this partial-dislocation strain-relaxation mechanism, we fabricated an $InP/In_{0.53}Ga_{0.47}As$ structure consisting of $In_{0.53}Ga_{0.47}$-As layers of thicknesses 56, 40, 28, 20, 14, 10, 7, 5, and 3.5 nm with intervening InP layers about 6 times thicker.

After cation homogenization by Zn diffusion, the structure became approximately $In_{0.94}Ga_{0.06}P/In_{0.94}Ga_{0.06}As$. The lattice mismatch is 3.2% and the conventional theory[3] for uncapped layers would predict a critical thickness of ~6 nm. We found that As layers with thickness equal to or smaller than 10 nm remain defect free. The 14-nm As layer exhibits a low density of {111} microtwins. As layers of thickness 20 nm or more are faulted heavily with microtwins and other defects, and the lattice is almost completely relaxed as revealed by electron diffraction. We also prepared specimens with AlAs layers of various thicknesses embedded in InP. The lattice mismatch is 3.5% and a critical thickness of ~5 nm is expected[3] for uncapped layers. We found that AlAs layers 2 and 3 nm thick are defect free while those 6 nm thick and thicker are heavily faulted. The 4-nm-thick AlAs layer exhibits {111} microtwins spaced microns apart, similar to that shown in Fig. 2. Details of this analysis will be presented elsewhere.

In summary, the existing theoretical calculations[3-9] for predicting the critical layer thickness are all based on perfect dislocations. Our experimental observations revealed that, in embedded strained layers near their critical thicknesses, the predominant strain-relaxation mechanism is the formation of partial dislocations. Our preliminary energy analysis indicates that the formation of partial dislocations is a more effective strain-relaxation channel for materials with small stacking-fault energy. Therefore, the existing theories should be modified to include this partial-dislocation relaxation mechanism. Partial dislocations result in stacking faults and microtwins which are detrimental to transport and optical properties and therefore limit the useful thicknesses of strained layers in device applications.

[1]F. C. Frank and J. H. van der Merwe, Proc. Roy. Soc. London A **198**, 216 (1949).

[2]J. H. van der Merwe, J. Appl. Phys. **34**, 117 (1963); **34**, 123 (1963).

[3]J. W. Matthews and A. E. Blakeslee, J. Cryst. Growth **27**, 118 (1974); **29**, 273 (1975).

[4]J. W. Matthews, J. Vac. Sci. Technol. **12**, 126 (1975).

[5]J. W. Matthews, S. Mader, and T. B. Light, J. Cryst. Growth **32**, 265 (1976).

[6]R. People and J. C. Bean, Appl. Phys. Lett. **47**, 322 (1985).

[7]B. W. Dodson and J. Y. Tsao, Appl. Phys. Lett. **51**, 1325 (1987); **52**, 852 (1988); **53**, 848 (1988).

[8]B. W. Dodson, Appl. Phys. Lett. **53**, 394 (1988).

[9]R. H. Miles and T. C. McGill, J. Vac. Sci. Technol. B **7**, 753 (1989).

[10]S. A. Schwarz, P. Mei, T. Venkatesan, R. Bhat, D. M. Hwang, C. L. Schwartz, M. Koza, L. Nazar, and B. J. Skromme, Appl. Phys. Lett. **53**, 1051 (1988).

[11]D. M. Hwang, S. A. Schwarz, P. Mei, R. Bhat, T. Venkatesan, L. Nazar, and C. L. Schwartz, Appl. Phys. Lett. **54**, 1160 (1989).

[12]S. A. Schwarz, P. Mei, D. M. Hwang, C. L. Schwartz, T. Venkatesan, C. J. Palmstrom, N. G. Stoffel, and R. Bhat, Mater. Res. Soc. Symp. Proc. **144**, 233 (1989).

[13]S. A. Schwarz, D. M. Hwang, P. Mei, C. L. Schwartz, J. Werner, N. G. Stoffel, R. Bhat, C. Y. Chen, T. S. Ravi, and M. Koza, J. Vac. Sci. Technol. A **8**, 2997 (1990).

[14]J. P. Hirth and J. Lothe, *Theory of Dislocations* (Wiley, New York, 1982), pp. 308 and 315.

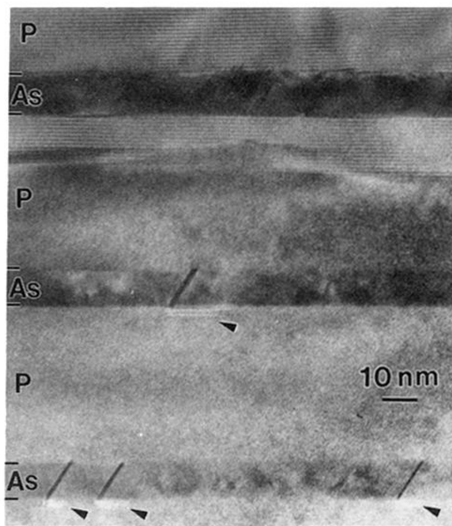


FIG. 1. TEM bright-field image taken along the $[1\bar{1}0]$ direction of an $InP/In_{0.53}Ga_{0.47}As$ superlattice after a 600 °C 1-h $Zn_3As_2$ treatment in a sealed ampoule. This micrograph shows a sharp front of $Zn_3P_2$ with 0.8-nm × 1.2-nm lattice fringes and the existence of $Zn_3P_2$ islands beyond the front as pointed by arrows. Adjacent to each $Zn_3P_2$ island is a microtwin spanning the 10-nm As layer.

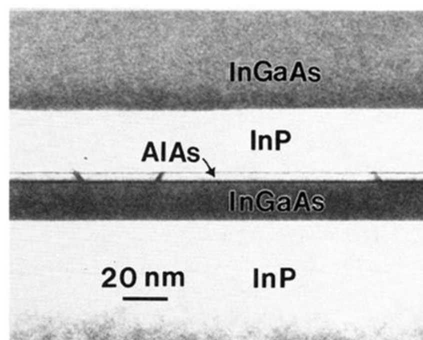


FIG. 2. TEM dark-field image taken along the $[1\bar{1}0]$ direction of a 5-nm AlAs layer embedded between InP and $In_{0.53}$-$Ga_{0.47}As$. Microtwins spanning the AlAs layer are observable.

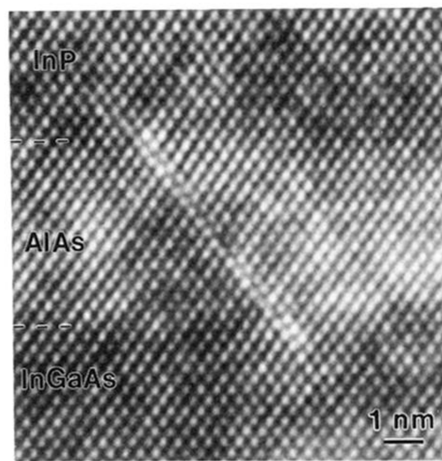


FIG. 3. High-resolution lattice image for the AlAs layer shown in Fig. 2. It shows an intrinsic stacking fault which can also be regarded as a monolayer-thick microtwin.